Analysis of High Frequency AC Link Isolated Three Port Resonant Converter for UAV Applications

Erdem Asa[1], Kerim Colak[2], Dariusz Czarkowski[3], Burak Ozpineci[1]
[1]Oak Ridge National Laboratory, National Transportation Research Center, Tennessee, USA
[2]Hevo Power Inc., New York, USA
[3]New York University, Tandon School of Engineering, New York, USA

Abstract — **A high frequency AC link isolated three port semi-bridgeless resonant converter is analyzed for unmanned aerial vehicle (UAV) applications in this study. The proposed topology is established by replacing rectifier lover diodes with synchronous switches. A phase shifted pulse width modulation (PS-PWM) technique adjusts bi-directional power flow between ports. Proposed control technique provides high efficiency by reducing switching losses with zero voltage switching (ZVS) and zero current switching (ZCS) in a wide power range regulation. Compared to integrated PWM converters in a bi-directional mode, the proposed topology reduces the number of converter stages and allows centralized control at high operating frequency. Theoretical and experimental results demonstrate the feasibility and effectiveness of the proposed converter at a full power of 500 W in laboratory conditions.**

Keywords— UAV, drone, battery, three-port, bi-directional, resonant, converter, power, energy, conversion.

I. INTRODUCTION

Unmanned aerial vehicles (UAVs) are widely used by profit or non-profit commercial and defense platforms where they can land or take off vertically for ground monitoring, security, powerline inspection, aid rescue after disasters, last mile delivery, etc [1]-[3]. Longer flight time at a low equipment cost is the main challenge for these applications [4]. Fuel engine propulsion machines result in load fluctuation due to narrow peak efficiency range and suffer low energy proficiency at low power. Although, energy storage systems are crucial in avionic applications, full electrical propulsion systems cannot afford long flight duration because of their limited storage densities, higher weight [5]-[6]. Consequently, hybrid propulsion systems with fuel propulsion engine paired with a dc machine / generator and energy storage systems in series, parallel, or series-parallel combinations has been attractive for UAV platforms. Considering maximum flight time, a series hybrid propulsion system provides maximum energy efficiency running the engine at an optimum efficiency to drive the electric propulsion machine and / or store the energy in battery as shown in Fig. 1. Energy conversion between source, load, and battery is usually provided in a bi-directional mode using isolated or non-isolated PWM dc / dc converters. Hard-switching causes high switching losses at high operating frequencies and typically requires a snubber or active clamp circuits across the switches. Resonant topologies are convenient converters for high operating frequency applications because of their zero-current (ZCS) or zero-voltage switching (ZVS) through the entire load range. Three port resonant converters might be useful to integrate energy sources with the battery and load rather than using a converter in each stage. The advantages of multi-port converters are high system efficiency, quick dynamic response, less passive components, centralized control, and high-power capability.

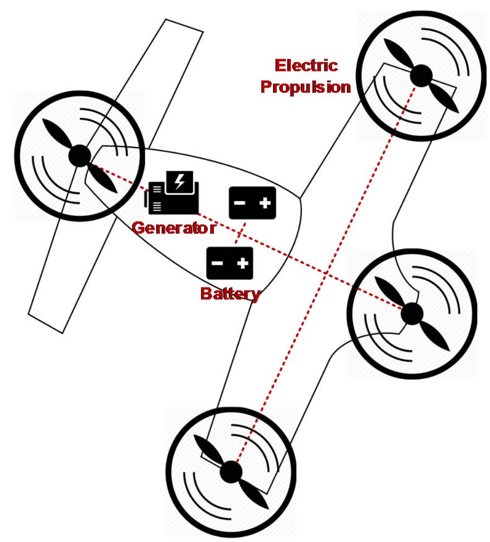

Fig. 1. Series hybrid propulsion UAV.

Several different three-port resonant converter topologies have been demonstrated in the literature [7]-[12]. Phase shift modulated interleaved three port series resonant converter which is connected to the grid through an additional inverter is described at constant operating frequency with a full-bridge rectifier in [7]. In order to optimize the parallel resonant inverter synchronization, a novel phase shift PWM technique is suggested for high frequency multi-port applications in [8].

Phase and magnitude control are achieved independently in steady state. A high frequency three-port isolated series resonant converter is introduced by using single three-winding transformer through active full bridges in [9]. Bi-directional energy conversion can be managed between active ports with a centralized control. Real-time power management of energy sources is presented using bi-directional isolated three-port resonant converter in [10]. The proposed parallel resonant converter can regulate multiple sources and loads with different voltage and current levels. Multiple port CLL resonant converter is introduced with asymmetrical PWM technique in [11]-[12], phase shift in [13], and hybrid regulation of phase shift and asymmetrical PWM in [14]-[15].

In this study, an isolated three port semi-bridgeless high frequency AC link resonant converter as shown in Fig. 2 is investigated for UAV applications. Phase shift modulation controls power regulation between inverter ports and synchronous active switches in a bi-directional mode. The proposed three port converter structure provides soft switching ZVS and ZCS at high operating frequencies in a wide input voltage range, output voltage range, and for varying load characteristics. Considering an air-gapped transformer in an LLC resonant converter, the CLL resonant circuit is an appropriate topology to use toroidal core transformer since provides high efficiency and less magnetic losses without any air gap. Toroidal core transformer with parallel inductor is used to reduce magnetic losses and design easier in this work. Due to large magnetizing inductance, this structure also ensures to drive load active switches easier that the current in each port is almost in phase. Without using any additional converter stages, the power can be directed between ports from source to battery and load, source to battery, and battery to load. The central controller can be used instead of using individual controllers for each port without the need for communication devices. Theoretical and simulation analysis of the system is validated with experimental results by testing a 500 W prototype in the laboratory conditions.

II. The Circuit Model and Theoretical Study of The Proposed Converter

The proposed isolated three port resonant converter with semi-bridgeless active rectifier circuit topology is shown in Fig. 2. It consists of two separate half-bridge resonant inverters with capacitors C_{P1}, C_{P2}, parallel inductances L_{P1}, L_{P2}, isolated transformers T_1, T_2, and single-phase semi-bridge active rectifier, in which two diodes D_1, D_2 in the upper and two FETs S_5, S_6 with anti-parallel diodes in the lower part. The phase shift angle controls the power flow and output by switching primary side half bridge inverters and secondary lower FETs.

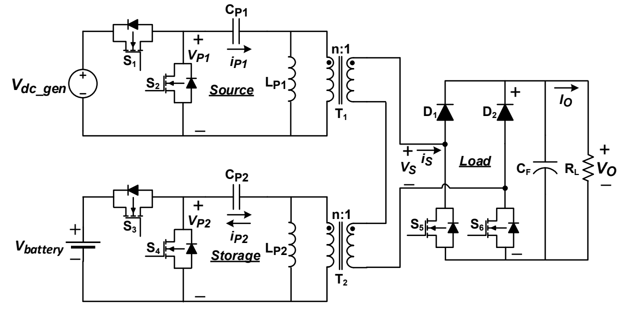

Fig. 2. The proposed isolated three port resonant converter.

By using the fundamental harmonic approximation (FHA), the equivalent circuit model and simplified model of the proposed system are shown in Fig. 3(a) and Fig. 3(b). The equivalent circuit parameters in Fig. 3(a) consist of the input voltage source V_{P1}, V_{P2}, the equivalent load impedance from the primary side Z_i and transformer model L_{T1}, L_{T2}, where $L_{T1}=\{L_{KP1}+L_{KS1}{*}\}$, $L_{T2}=\{L_{KP2}+L_{KS2}{*}\}$ as shown in Fig. 3(b).

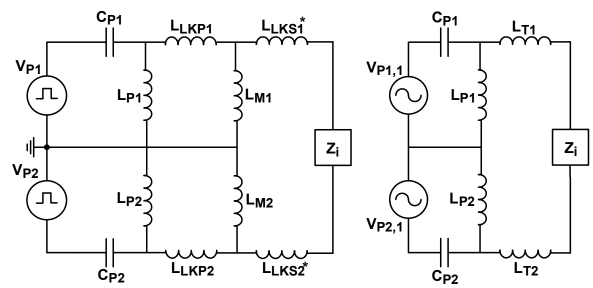

a) b)

Fig. 3. The proposed converter a) equivalent circuit, b) simplified model.

Each half bridge inverter can be described using FHA analysis,

$$v_{P1}(t) = \begin{cases} V_{dc\_gen}, < \omega t \leq \pi \\ 0, \quad \pi < \omega t \leq 2\pi \end{cases} \tag{1}$$

$$v_{P2}(t) = \begin{cases} V_{battery}, -\phi < \omega t \leq \pi - \phi \\ 0, \quad \pi - \phi < \omega t \leq 2\pi - \phi \end{cases} \tag{2}$$

where ϕ defines the phase shift function between the inverter ports. The fundamental components of the voltages $v_{P1,1(t)}$, $v_{P2,1(t)}$ can be specified in the phasor domain as

$$V_{P1,1} = \frac{2}{\pi} V_{source} \tag{3}$$

$$V_{P2,1} = \frac{2}{\pi} V_{battery} e^{j\phi} \tag{4}$$

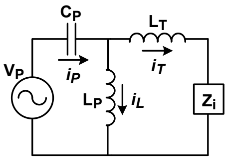

Fig. 4. The proposed converter one phase equivalent model.

The equivalent model can be simplified to one phase as shown in Fig. 4, where the input source voltage V_P=$V_{P1,1}$+$V_{P2,1}$, equivalent capacitor C_P=$C_{P1}C_{P2}/(C_{P1}+C_{P2})$, parallel inductor L_P=L_{P1}+L_{P2}, and transformer L_T=L_{T1}+L_{T2} can be defined. The equivalent impedance Z_i value is obtained for the inductive and capacitive modes as,

$$Z_i = \frac{8n^2R_L}{\pi^2}\sin^3\left(\frac{\beta}{2}\right)\left[\sin\left(\frac{\beta}{2}\right)+j\cos\left(\frac{\beta}{2}\right)\right]\ for\ inductive\ mode \quad (5)$$

$$Z_i = \frac{8n^2R_L}{\pi^2}\sin^3\left(\frac{\beta}{2}\right)\left[\sin\left(\frac{\beta}{2}\right)-j\cos\left(\frac{\beta}{2}\right)\right]\ for\ capacitive\ mode \quad (6)$$

where β is rectifier conduction angle, n and R_L are transformer turns ratio and load resistance of the converter, respectively. The system critical frequency ω_C, normalized frequency ω_n, and quality factor Q can be calculated as,

$$\omega_C = \frac{1}{\sqrt{L_P C_P}}, \omega_n = \frac{\omega_{sw}}{\omega_C} \quad (7)$$

$$Q = R_L\sqrt{\frac{C_{P1}}{L_{P1}}} \quad (8)$$

Using the above relationships, the voltage gain $|M_V|$ of the proposed converter can be shown as,

$$|M_V| = \left|\frac{V_O}{V_{P1,1}+V_{P2,1}}\right| = \left|\frac{2\sqrt{2}\sin^2\left(\frac{\beta}{2}\right)}{\pi\left[\frac{2}{j\omega_n Q}+\left(\frac{2Aj\omega_n}{Q}+B\right)\left(1-\frac{1}{\omega_n^2}\right)\right]}\right| \quad (9)$$

where A {=$L_T/(2L_P)$} is the ratio between transformer leakage and parallel connected inductance and B {=Z_i/R_L}.

III. THE POWER FLOW INVESTIGATION OF THE PROPOSED SYSTEM

The power flow regulation between input ports and output port is examined considering the equivalent circuit of Fig. 5. As seen from the figure, the system energy conversion analysis for two input ports have different sources but the same resonant converter parameters. The equivalent input voltages of the two input ports can be written as,

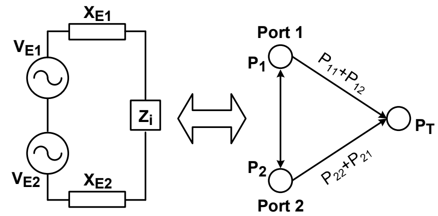

Fig. 5. The proposed converter power flow illustration.

$$V_{E1} = \frac{V_{P1,1}}{1-\frac{1}{\omega_n^2}} \quad (10)$$

$$V_{E2} = \frac{V_{P2,1}}{1-\frac{1}{\omega_n^2}} \quad (11)$$

and converter output impedance can be stated as

$$Z_L = Z_i + 2jX_E = |Z_L|e^{j\theta_L} \quad (12)$$

where Z_i can be described in real and imaginary parts as Z_i=R_i+jX_i, and X_E and θ_L can be written as,

$$X_E = \left[\frac{Z_r^2}{\frac{1}{j\omega_{sw}C_{P1}}+j\omega_{sw}L_{P1}}\right] + j\omega_n L_{T1} \quad (13)$$

$$\theta_L = \tan^{-1}\left[\frac{2X_E+X_i}{R_i}\right] \quad (14)$$

where two port characteristic impedance Z_r is equal to $\sqrt{L_{P1}/C_{P1}}$ and $\sqrt{L_{P2}/C_{P2}}$. The power equations can be derived from source to the output and between input ports as following,

$$P_{11} = \frac{|V_{E1}|^2}{|Z_L|^2}\frac{R_i}{2} \quad (15)$$

$$P_{12} = \frac{|V_{E1}||V_{E2}|}{2|Z_L|}\cos(\phi-\theta_L) \quad (16)$$

$$P_{22} = \frac{|V_{E2}|^2}{|Z_L|^2}\frac{R_i}{2} \quad (17)$$

$$P_{21} = \frac{|V_{E1}||V_{E2}|}{2|Z_L|}\cos(\phi+\theta_L) \quad (18)$$

The total output power is $P_T = P_{11} + P_{12} + P_{21} + P_{22}$. The power circulation between ports is illustrated for the two input source combinations in Fig. 6 and Fig. 7, and for the output power in Fig. 8. As seen from the figures, the power can be regulated from main source to battery and / or load, and battery to load at a desired value by phase shift function ϕ between input ports and conduction angle β.

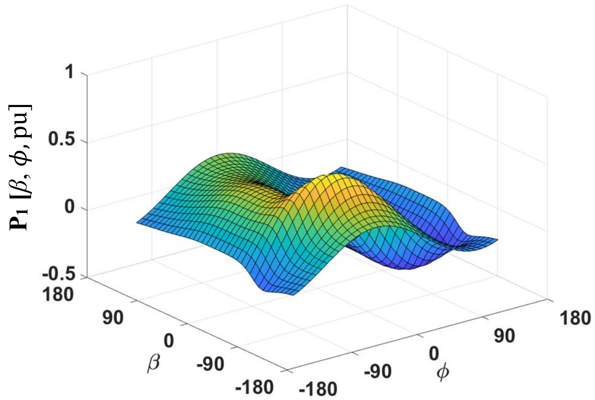

Fig. 6. The first input power with two input sources and conduction angle β and phase shift angle ϕ for the main source.

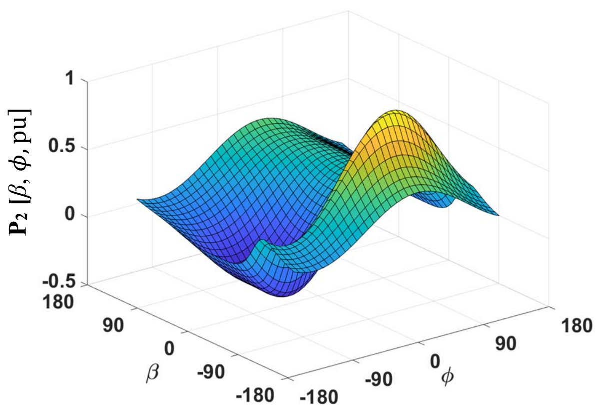

Fig. 7. The second input power with two input sources and conduction angle β and phase shift angle ϕ for the battery source.

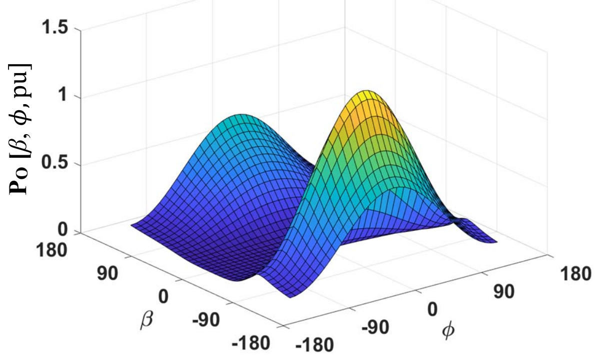

Fig. 8. The output power with two input sources and conduction angle β and phase shift function ϕ for the output load.

IV. Experimental Results

The proposed system is experimented for 500 W, 60 V-60 V input voltages, and 0-100 V / 0-5 A output rating in the laboratory conditions. The converter parameters are summarized in Table I. The converter input and output voltage / current waveforms are measured with Rigol DS1054Z oscilloscope. And, the input and output power values are recorded by Yokogawa PZ4000.

TABLE I - THE PROPOSED CONVERTER PARAMETERS

Symbol	Parameter	Values
V_P	dc input voltages	60 V - 60 V
V_O	dc output voltage range	0 - 100 V
I_O	output current range	0 - 5 A
P_O	rated power	500 W
C_P	resonant capacitor	60 nF
L_P	parallel inductance	24 uH
L_{lk}	transformer leakage	30 uH
L_M	transformer magnetizing	780 uH
f	operating frequency	190 kHz
D	transformer core	OP48020EC
L	transformer shape	Toroid
n	transformer turn ratio	1:1
S	main switch	IRFP4227PbF
D	rectifier diode	DSEI2X101
t_{dead}	dead time	300 ns

In order to show the resonant tank primary and secondary signals, selected voltage and current waveforms are given for phase shift function ϕ *(=150º, 120º, and 90º)*, conduction angle β *(=110º, -90º, and -170º)*, and different load conditions *(=10 Ω, 20 Ω, and 30 Ω)* in Fig. 9. The system control angle between input ports and between output port manages the active switches conduction angle β in condition of different loads as seen from the figures. In this way, energy conversation can be achieved between input and output ports. The input and output power flow between theoretical and experimental results are shown when β at *90º*, *120º*, *150º* and ϕ at *-180º to 180º (polar axis)* for different load conditions in Fig. 10. The different input and output power series can be reached by the proper phase angle between ports at the constant operating frequency. As seen from the figures, a certain power between converter ports can be obtained at different phase shift values under different loads. The power flow between the sources is also possible with the controller angle. The performance of the proposed system is given in Fig 11 as the same conditions in the power flow analysis. As seen from the results, the maximum efficiency is obtained around 96% at half of the load. In results of experimental analysis show that ZVS and ZCS boundary conditions are important to provide high efficiency during energy flow between converter ports. Thus, the same power level can be achieved with the different efficiency results at different ϕ and β values as seen from the results.

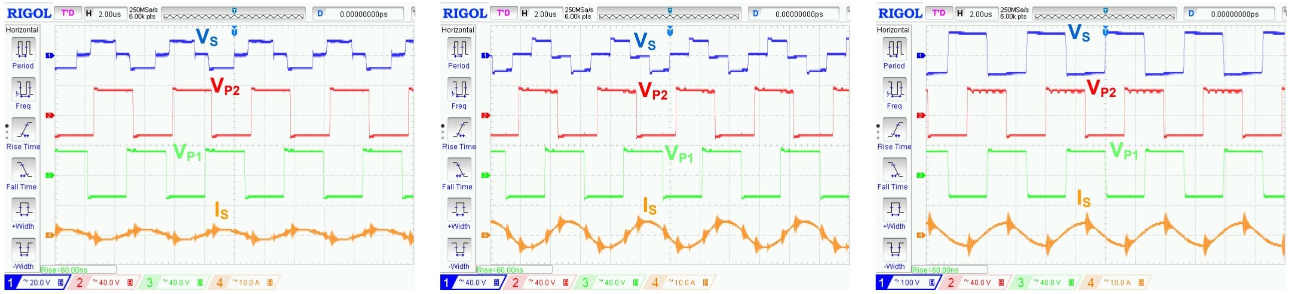

a) ϕ=150° and β=110° for 10 Ω b) ϕ=120° and β=-90° for 20 Ω c) ϕ=90° and β=-170° for 30 Ω

Fig. 9. Primary side resonant tank voltages V_{P1} and V_{P2}, secondary side voltage V_S, current I_S waveforms.

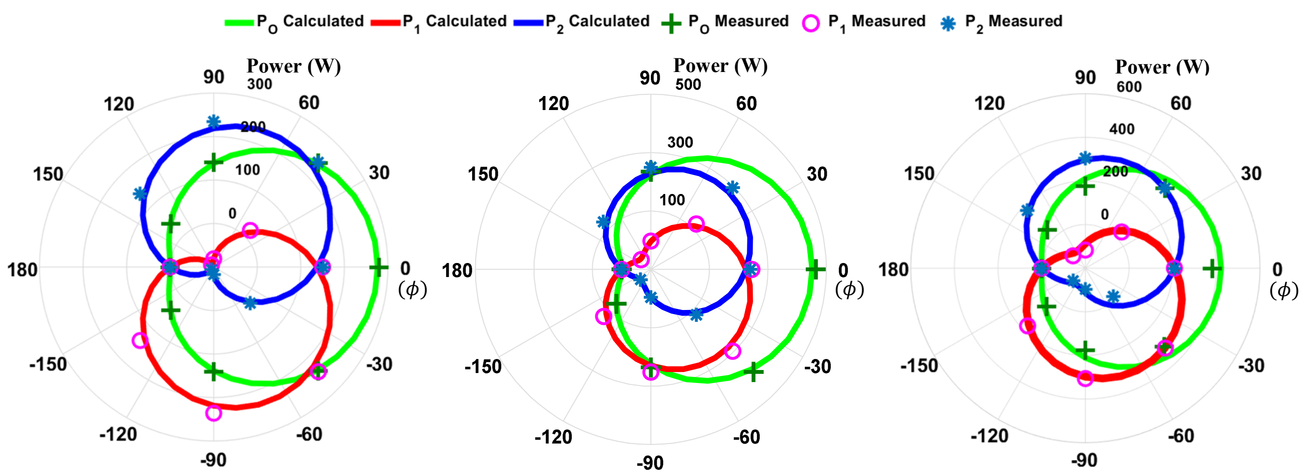

a) 10 Ω and β at *-150°* b) 20 Ω and β at *-120°* c) 30 Ω and β at *-90°*

Fig. 10. Input and output power characteristics with ϕ *(polar axis -180° to 180°)* and β at the different load conditions.

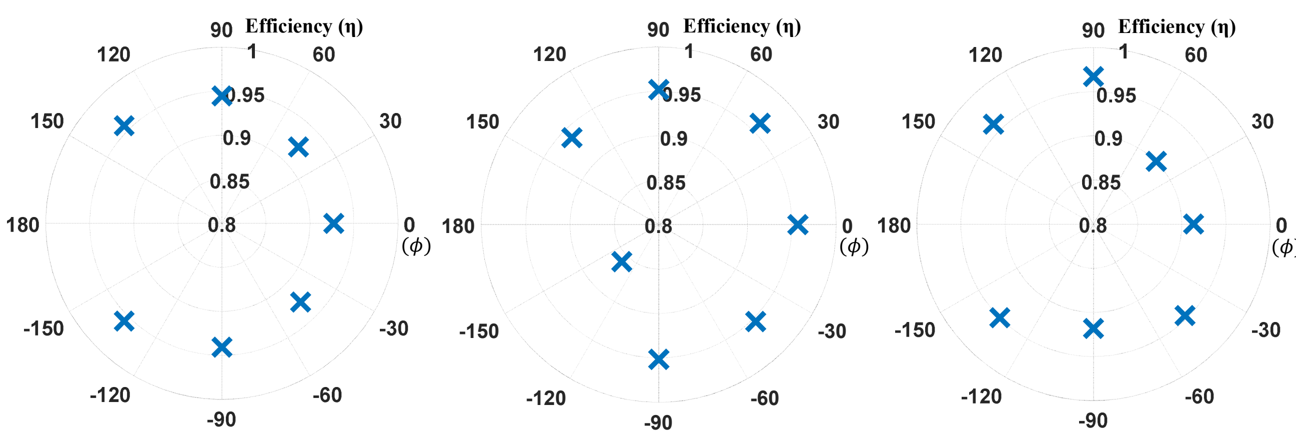

a) 10 Ω and β at *-150°* b) 20 Ω and β at *-120°* c) 30 Ω and β at *-90°*

Fig. 11. The proposed system efficiency characteristic with ϕ *(polar axis -180° to 180°)* and β at the different load conditions.

V. CONCLUSIONS

In this paper, a new isolated three port resonant converter is presented for UAV applications. With the proposed secondary side active switches, a wide power circulation can be achieved between ports by using the phase shift control angle. Novel converter topology has reduced number of active stages comparing to the existing solutions. The converter model theoretical analysis is given using FHA and simplified circuit analysis. The system transfer function is derived by providing an equivalent circuit of the topology. By using two different balanced input dc voltage combinations, experimental results are obtained with the maximum 96% efficiency. The source voltages are 60 V-60 V and output voltage and current ranges are 0 to 100 V / 0 to 5 A, respectively. The experimental results prove that the proposed system provides a wide power regulation with the phase shift angle control of each converter ports. Another advantage of the system considering the high-power capability of the converter that it can be used to split the power among ports in desired proportions.

REFERENCES

[1] M. Aghaei, F. Grimaccia, C. A. Gonano, S. Leva, "Innovative automated control system for PV fields inspection and remote control," IEEE Trans. Ind. Electron., vol. 62, no. 11, pp. 7287-7296, Nov. 2015.

[2] J. J. Cooley, P. Lindahl, C. L. Zimmerman, M. Cornachione, G. Jordan, S. R. Shaw, S. B. Leeb, "Multiconverter system design for fuel cell buffering and diagnostics under UAV load profiles," IEEE Trans. Power Electron., vol. 29, no. 6, pp. 3232-3244, Jun. 2014.

[3] J. M. Arteaga, S. Aldhaher, G. Kkelis, C. Kwan, D. C. Yates, P. D. Mitcheson, "Dynamic capabilities of multi-MHz inductive power transfer systems demonstrated with batteryless drones," IEEE Trans. Power Electron., vol. 34, no. 6, pp. 5093-5104, Jun. 2019.

[4] E. Bertran, A. Sànchez Cerdà, "On the trade-off between electrical power consumption and flight performance in fixed-wing UAV autopilots," IEEE Trans. Veh. Technol., vol. 65, no. 11, pp. 8832-8840, Nov. 2016.

[5] S. Aldhaher, D. C. Yates, P. D. Mitcheson, "Load-Independent Class E/EF Inverters and Rectifiers for MHz-Switching Applications," IEEE Trans. Power Electron., vol. 33, no. 10, pp. 8270-8287, Oct. 2018.

[6] J. Zhou, B. Zhang, W. Xiao, D. Qiu, Y. Chen, "Nonlinear parity time symmetric model for constant efficiency wireless power transfer: application to a drone in flight wireless charging platform," IEEE Trans. Ind. Electron., vol. 66, no. 5, pp. 4097-4107, May 2019.

[7] I. J. Pitel, "Phase-modulated resonant power conversion techniques for high-frequency link inverters," IEEE Trans. Ind. Appl., vol. IA-22, no. 6, pp. 1044-1051, Nov. 1986.

[8] J. Liu, K. W. E. Cheng, J. Zeng, "A unified phase-shift modulation for optimized synchronization of parallel resonant inverters in high frequency power system," IEEE Trans. Ind. Electron., vol.61, no.7, pp.3232-3247, Jul. 2014.

[9] H. Krishnaswami, N. Mohan, "Three-port series-resonant DC–DC converter to interface renewable energy sources with bidirectional load and energy storage ports," IEEE Trans. Power Electron., vol. 24, no. 10, pp. 2289-2297, Oct. 2009.

[10] J. Zeng, W. Qiao, L. Qu, "An isolated three-port bidirectional dc-dc converter for photovoltaic systems with energy storage," IEEE Trans. Ind. Appl., vol.51, no.4, pp.3493-3503, Jul./Aug. 2015.

[11] D. J. Tschirhart, P. K. Jain, "A CLL resonant asymmetrical pulsewidth-modulated converter with improved efficiency," IEEE Trans. Ind. Electron., vol.55, no.1, pp.114-122, Jan. 2008.

[12] K. Colak, E. Asa, M. Bojarski, D. Czarkowski, "Asymmetrical duty-cycle control of a novel multi-port CLL resonant converter," IEEE Applied Power Electronics Conference and Exposition, Charlotte, NC, 2015, pp. 3019-3024.

[13] E. Asa, K. Colak, D. Czarkowski, "Analysis of a novel interleaved CLL resonant converter for EV battery charger applications," IEEE Energy Conversion Congress and Exposition, Pittsburgh, PA, 2014, pp. 2031-2036.

[14] S. H. Ryu, D. H. Kim, M. J. Kim, J. S. Kim, B. K. Lee, "Adjustable frequency-duty-cycle hybrid control strategy for full-bridge series resonant converters in electric vehicle chargers," IEEE Trans. Ind. Electron., vol.61, no.10, pp.5354-5362, Oct. 2014.

[15] E. Asa, K. Colak, M. Bojarski, D. Czarkowski, "Asymmetrical Duty-Cycle and Phase-Shift Control of a Novel Multiport CLL Resonant Converter," in IEEE Journal of Emerging and Selected Topics in Power Electronics, vol. 3, no. 4, pp. 1122-1131, Dec. 2015.